Design of a robotic platform for hybrid wind tunnel experiments of floating wind farms

Journal of Physics: Conference Series **2767** (2024) 042008 doi:10.1088/1742-6596/2767/4/042008

Design of a robotic platform for hybrid wind tunnel experiments of floating wind farms

A. Fontanella[1], G. Palombini[1], A. Piffer[1], H. Giberti[2], M. Belloli[1]

[1] Dept. of Mechanical Engineering, Politecnico di Milano, via La Masa 1, 20156 Milano, Italy.
[2] Dept. of Electrical, Computer and Biomedical Engineering, Università degli Studi di Pavia, via Adolfo Ferrata 5, 27100 Pavia, Italy.

E-mail: alessandro.fontanella@polimi.it

Abstract. Wind tunnel experiments incorporating factors like realistic ambient wind conditions, merging of multiple wakes, and active wake controls are needed to understand and improve modeling of floating wind farms. A key technology for this kind of experiments is the robotic system emulating the wind turbine motion. This article addresses the design of a robotic platform with three degrees-of-freedom (surge, pitch, and yaw) specifically tailored for wind tunnel experiments on floating wind farms. This robotic system aims to accurately reproduce the motion spectrum of floating wind turbines of 10-22MW and to simulate rotor-atmospheric wind interactions. The robotic platform has a compact design to be positioned in multiple units inside the wind tunnel and avoid disturbing the wake of the wind turbine on top of it. To achieve these goals, the wind turbine is partially integrated in the robotic platform that employs a parallel kinematic scheme and has all actuators close to the wind tunnel floor.

1. Introduction

In recent years, the first utility-scale floating wind farms have been installed and others are expected to go online in the next future. However, the effects of large motions allowed by the high compliance of the floating foundation on wind turbine wake and on wake-flow control strategies are still poorly understood [1]. The impact of surge motion on the near wake of a 1:75 scale model of a 10MW turbine is investigated in the wind tunnel experiment of [2] and measurements are compared to numerical codes of different fidelity in [3, 4]. Results of these studies should be extended including additional physics that are important for wake development, such as realistic ambient wind conditions (e.g., turbulence and vertical shear), merging of multiple wakes, propagation of wakes to distances meaningful for commercial wind farms, and the presence of active wake controls.

Scale mode testing of floating wind turbines is complicated by the need to reproduce at the same time aerodynamic and hydrodynamic phenomena which are governed by different physics. One solution to this problem is represented by the hybrid methodology: the wind turbine is a physical scale model with realistic aerodynamic performance and control capabilities, whereas the platform motion due to hydrodynamic loads is emulated with the combination of measurements, a simulation model, and a robotic device [5]. This approach is advantageous for wake-related studies because it favors an accurate representation of the wind domain and hence of wind turbine wakes.

A key enabling technology for hybrid wind tunnel experiments is the robotic system moving the wind turbine. The objective of this work is to provide information about the design of a robotic platform for hybrid wind tunnel experiments of wake interactions and flow control in floating wind farms. The robot has three degrees-of-freedom: the wind turbine is moved in the surge and pitch directions and has nacelle-yaw actuation. Differently than other robotic devices used in wind tunnel experiments (e.g., [2, 6]) the one of this work is designed to comply with requirements of floating wind farm flow studies: the robot reproduces accurately the motion of multi-megawatt floating wind turbines at a fraction of their size; it has compact dimensions to minimize disturbances of the wind turbine wake and to install multiple robot-wind turbine units in the wind tunnel; it correctly positions the wind turbine hub within the wind tunnel boundary layer to mimic the interaction between rotor and atmospheric wind.

2. Definition of input data

The input data for the robot design are the specifications of the full-scale turbines to be emulated in the wind tunnel (Sect. 2.1), the scaling laws (Sect. 2.2), and the aerodynamic loads of a model scale rotor compatible with the robot size (Sect. 2.3).

2.1. Full-scale wind turbines of reference

The robotic platform is thought to enable experiments of wind farms aerodynamics considering plants with turbines of different rating. Robot specifications are drawn making reference to three wind turbine concepts: the DTU 10MW [7], the IEA 15MW [8], and the IEA 22MW [9], whose key parameters are summarized in Table 1. The hub height and rotor diameter increase with the power rating, of 50% and 60% respectively, passing from the 10MW to the 22MW. The wind turbines have similar wind speed operating range, but the 10MW has lower design TSR and higher rated rotor speed compared to the 15MW and 22MW.

Table 1. Key parameters of the wind turbines considered as reference in the robot design.

Parameter	10MW	15MW	22MW
Cut-in, rated, cut-off wind speeds [$\mathrm{m\,s^{-1}}$]	4, 11.4, 25	3, 10.6, 25	3, 10.6, 25
Rotor diameter [m]	178.4	242	284
Hub height [m]	119	150	182
Design TSR [−]	7.5	9.0	9.15
Rated rotor speed [rpm]	9.6	7.6	7.06
Rated mechanical power [MW]	10.6	15.7	23.1

2.2. Scaling laws

Scaling laws for wind tunnel experiments on wind turbines based on the hybrid methodology use a geometric scale factor λ_L and a scale factor for velocities λ_v, expressing the ratio between model-scale and full-scale quantities.

λ_v is defined comparing the wind speed operating range of the wind turbines, reported in Table 1, with the wind speed range of the wind tunnel. The maximum wind speed reached when reproducing a boundary layer inflow is 15 $\mathrm{m\,s^{-1}}$, thus we choose $\lambda_v = 1{:}2$ to cover all functioning conditions of the wind turbines.

λ_L is set to reproduce at a scale the interaction between rotor and atmospheric boundary layer that we assume to be governed by the shape of the vertical profiles of mean wind speed and

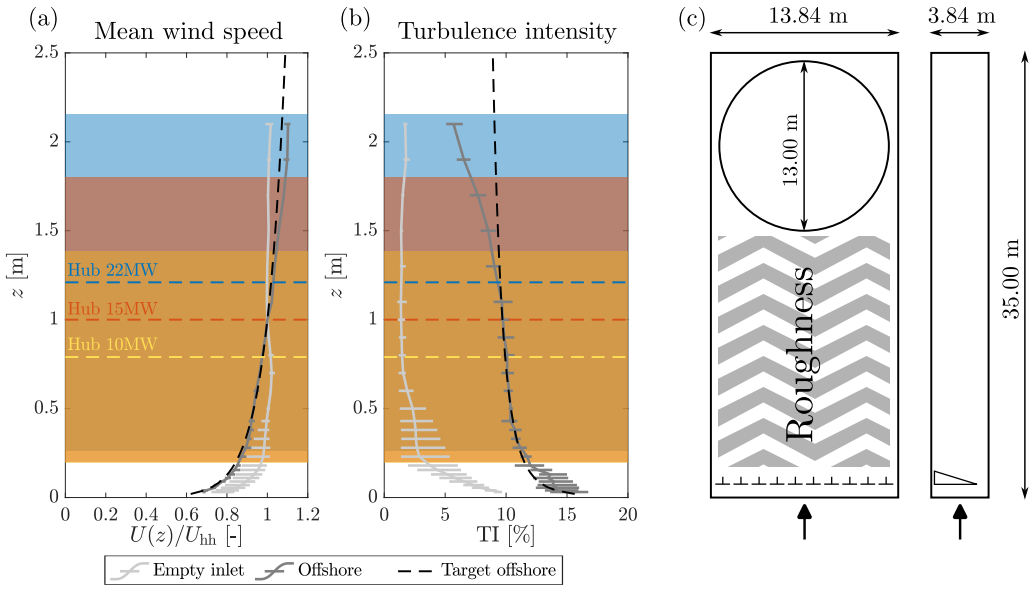

Figure 1. Geometric constraints for the robot design. **(a, b)** dimensions of 1:150 scale rotors of the 10MW, 15MW, and 22MW wind turbines, represented by colored areas, are compared to wind profiles generated at the POLIMI wind tunnel (empty inlet corresponds to smooth flow); error bars are the min/max across the test section and "Target offshore" is the typical logarithmic profile for an offshore site. **(c)** Main dimensions of the wind tunnel test section; the dashed area is occupied by roughness elements and it is used to shape wind characteristics.

turbulence intensity. The wind tunnel can reproduce typical wind profiles at a scale $\lambda_L = 1{:}150$ and this is exemplified in Fig. 1 for an offshore wind condition with a model-scale roughness length of 5.91mm. With $\lambda_L = 1{:}150$, profiles created in the wind tunnel match well the target prescribed by standards across the rotor disk of the 10MW and 15MW scale models; only for the 22MW the turbulence intensity is lower than expected in the upper portion of the rotor.

2.3. Wind turbine aerodynamic loads

Aerodynamic loading on the rotor is modeled with the thrust force and rotor torque at the hub. These are computed from the power and thrust coefficients (C_P and C_T, respectively) of the DTU 10MW scaled rotor that is designed and characterized experimentally in [10]. The scaled rotor reproduces the distributed normal loading of the DTU 10MW blade making use of the SD7032 low-Reynolds airfoil and ad-hoc designed chord and twist distributions. It has a maximum power coefficient $C_{P,\text{model}} = 0.39$ at TSR $= 7.5$ and the corresponding thrust coefficient is $C_{T,\text{model}} = 0.88$. Experimental testing with rotor misalignment has shown the aerodynamic torque on the yaw axis is 0.3Nm with a 30° nacelle-yaw angle.

Scale model rotors of the 15MW and 22MW have not been designed yet. Thus, we assume they have the same $C_{P,\text{model}}$ and $C_{T,\text{model}}$ of the 10MW scaled rotor, but at their design TSR instead of TSR $= 7.5$. The maximum aerodynamic yaw torque is assumed to be 0.3Nm for all rotors.

3. Design requirements

General requirements for the design of the robotic platform are:

- reproduce the platform surge and pitch motions of floating wind turbines. Motion in these directions influences the rotor apparent wind speed and has the strongest effect on the

aerodynamic response;

- have an actuation mechanism to control the nacelle yaw. This degree of freedom is used to actuate wake steering in wind farm control strategies; moreover, dynamic yaw motion due to wave excitation may influence the wake meandering;
- place the wind turbine hub at the correct height from ground to reproduce the interaction with atmospheric wind (as shown in Fig. 1).

More specific requirements are defined concerning the surge, pitch, and yaw dynamic motions (Sect. 3.1) and the power generated by the wind turbine that has to be absorbed by its generator (Sect. 3.2), which will be integrated in the robot structure as we will explain later.

3.1. Motion requirements

Motion requirements are set in terms of maximum motion amplitude A_m for several values of motion frequency f_m. We examine two operating scenarios: sinusoidal motion and testing with simulation of stochastic waves. We use these scenarios to define different requirements for the robot. Sinusoidal motion is an idealized condition often used in experiments on floating wind turbine aerodynamics. In case of sinusoidal movements representative of previous wind tunnel studies, the maximum f_m and A_m, and hence the maximum velocities and accelerations, are demanding and set the force and operating frequency requirements for the robot actuators. In normal operating conditions, floating wind turbines are likely to be exposed to mild waves resulting in smaller platform movements than those considered in sinusoidal motion tests. Due to the scaling we adopted, these motions are hard to measure and control in the wind tunnel environment and they set the requirements for the accuracy of the robot motion sensors.

3.1.1. Sinusoidal motion. The platform motion along one direction ξ is

$$\xi(t) = A_{\mathrm{m},0} + A_\mathrm{m} \sin(2\pi f_\mathrm{m} t + \varphi_\mathrm{m}) \,, \tag{1}$$

where $A_{\mathrm{m},0}$ is the static component and φ_m is the motion phase. In experiments with sinusoidal motion it is common practice to put into relation A_m and f_m by means of two parameters. One is the rotor reduced frequency

$$f_\mathrm{r} = \frac{f_\mathrm{m} D}{U} \,, \tag{2}$$

where D is the wind turbine diameter and U the undisturbed wind speed. The other is the apparent wind speed due to motion ΔU. For the three motion directions of the robot we have:

- surge: the apparent wind is uniform across the rotor area and is equal to $\Delta U = 2\pi f_\mathrm{m} A_\mathrm{m}$;
- pitch: we decide to control the wind speed at hub and $\Delta U_\mathrm{hub} = 2\pi f_\mathrm{m} A_\mathrm{m} r_\mathrm{hub}$, where r_hub is the hub distance from the pitch rotation point;
- yaw: we control the apparent wind speed at the rotor edge and $\Delta U_\mathrm{r} = 2\pi f_\mathrm{m} A_\mathrm{m} R$, where R is the rotor radius.

Motion requirements are visualized in Fig. 2 and are obtained setting $f_{\mathrm{r,max}} = 1$ and $\Delta U_\mathrm{max} = 0.5\mathrm{m\,s^{-1}}$, which is representative of previous experimental research [11]. For every $U \in [U_{\mathrm{cut-in}}\lambda_v, U_{\mathrm{cut-off}}\lambda_v]$ the motion frequency is $f_\mathrm{m} = U f_{\mathrm{r,max}} D^{-1}$. The corresponding amplitude is: for surge $A_\mathrm{m} = \Delta U_\mathrm{max}(2\pi f_\mathrm{m})^{-1}$; for pitch $A_\mathrm{m} = \Delta U_\mathrm{max}(2\pi f_\mathrm{m} h_\mathrm{hub})^{-1}$; for yaw $A_\mathrm{m} = \Delta U_\mathrm{max}(2\pi f_\mathrm{m} R)^{-1}$. From the expression of ΔU it follows the required motion amplitude decreases for increasing f_m. From Eq. 2 we have that the maximum frequency of motion is inversely proportional to the rotor diameter since the wind speed operating range is similar for the three turbines and it is 10.5Hz for the 10MW.

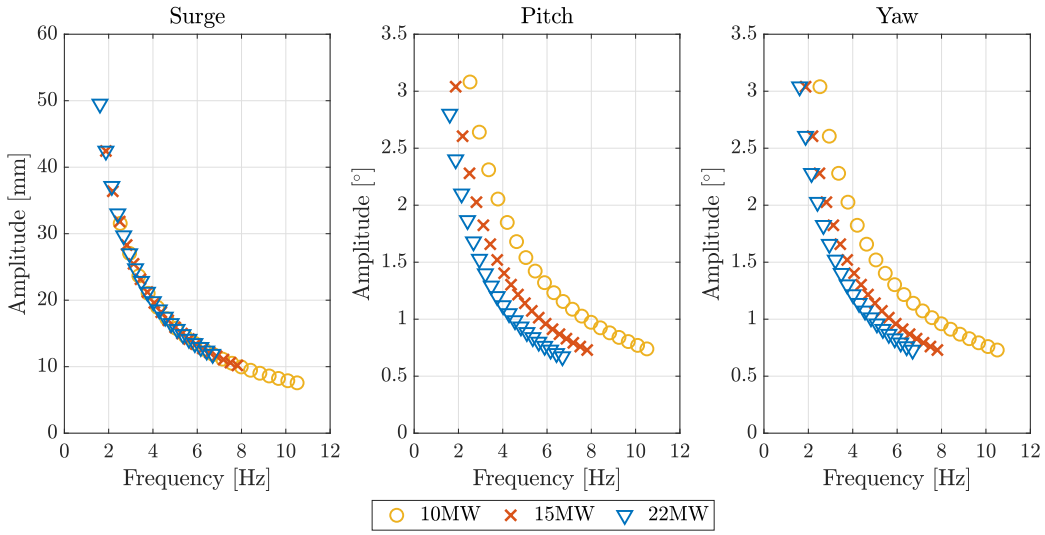

Figure 2. Motion requirements for the surge, pitch, and nacelle yaw degrees of freedom for prescribed motion tests.

3.1.2. Testing with stochastic waves. In this testing scenario, platform motion is obtained from a time-marching simulation of the platform response to stochastic waves excitation. The simulation can be run either offline or in real-time during testing with the hardware-in-the-loop approach [5].

Figure 3 shows the model-scale time series and spectra of the platform surge and pitch motions of a 10MW, 15MW, and 22MW floating wind turbines with an average wind speed of $10\,\mathrm{m\,s^{-1}}$, irregular waves of 1m of significant height and 7s of peak period that are representative of mild sea conditions. The 10MW has a hybrid spar–semi-submersible platform [12], the 15MW and 22MW are mounted on semi-submersibles [13]. The time series are computed in OpenFAST and are scaled according to the scaling rules of Sect. 2.2: platform surge is multiplied by λ_L, platform pitch is unchanged since it is a rotation, and the time vector is multiplied by $\lambda_L\lambda_v^{-1}$. The motion amplitude is confined to 1mm and 0.05°, which are significantly less than the requirements for sinusoidal motion tests. Motions spectra present a low-frequency peak near 1Hz, corresponding to the platforms rigid-body modes, and one around 9Hz, in proximity of the wave excitation band. The frequency range of interest, which is below 15Hz, includes these two peaks. In this range, the motion amplitude is 0.01-0.4mm for surge and 0.3-20m° for pitch (where m° is the unit for millidegrees).

3.2. Generator torque and power

The requirement for the generator is to provide the braking torque that counteracts the steady-state rotor torque at rated rotor speed. The rotor power is

$$P_\mathrm{r} = \frac{1}{2}\rho {U_\mathrm{r}}^3 A_\mathrm{r} C_{P,\mathrm{model}}\,, \tag{3}$$

where U_r and A_r are the scaled rated wind speed and rotor area of the three reference wind turbines, and $C_{P,\mathrm{model}} = 0.39$. The generator requirements for the three scale models are summarized in Table 2.

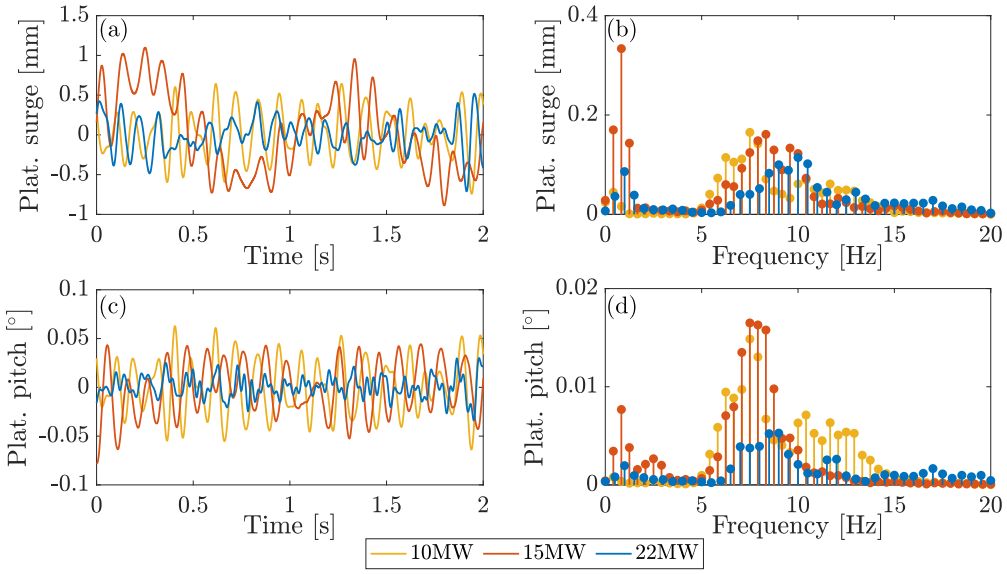

Figure 3. Motion requirements for the surge and pitch degrees of freedom in testing with stochastic waves. **(a, c)** time series. **(b, d)** spectra.

Table 2. Requirements for the generator for scale models of the 10MW, 15MW, and 22MW reference wind turbines.

Parameter	10MW	15MW	22MW
Rated rotor speed [rpm]	720	570	530
Rotor power [W]	49	72	100
Rotor torque [mNm]	653	1198	1798

4. Design process

Given the design requirements, it is clear the robot has to move at relatively high frequency, with high accuracy, in some cases reaching considerable accelerations (a sinusoidal surge motion of $A_\mathrm{m} = 10\mathrm{mm}$ and $f_\mathrm{m} = 10\mathrm{Hz}$ results in a peak acceleration of $40\mathrm{m\,s^{-2}}$). To meet these needs, the robot is configured as a parallel kinematic machine in which the links are joined in a closed sequence. This choice ensures a low sensitivity to backlashes in the joints and thus high positioning accuracy. Moreover, loads on the links are almost purely of axial nature leading to a structure that has high stiffness and low mass, which is beneficial for the robot dynamic performance.

To further improve stiffness and limit dimensions, the wind turbine has been partially integrated in the robot structure: the lower half of the tower is part of the kinematic chain and constitutes one of the robot links. Moreover, the wind turbine nacelle and generator are designed together with the rest of the robot components. In this way, the nacelle geometry and mass properties remain the same independently of the wind turbine rotor mounted on the robot and this has two positive consequences: the tower-top inertia properties are fixed and independent from the turbine rating, thus it is easier to integrate them in the robot design; the generator can be interfaced with the robot control hardware providing a unified control environment for all wind turbine degrees of freedom.

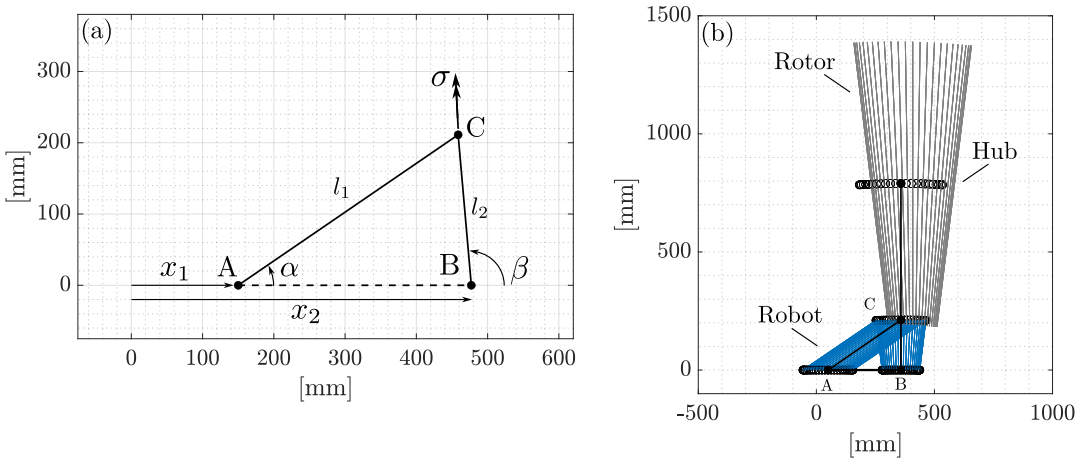

Figure 4. Kinematics of the robotic platform. **(a)** geometry of the robot. **(b)** work space of the robot and wind turbine with a prescribed surge-pitch motion.

4.1. Kinematic configuration

Figure 4 shows the kinematic topology of the robot. It is formed of two links (l_1 and l_2) and three joints (A, B, C) that lie in a vertical plane. Joints in A and B combine an actuated prismatic joint with a passive rotational one; C is a passive rotational joint connecting the two links. This kinematic configuration is selected because the actuators are near the ground, which reduces the overall dimensions of the upper part of the robot. Moreover, the robot has a streamlined configuration limiting disturbances introduced in the flow: the link l_1 is behind the turbine tower and the attachment point C is in proximity of the lower rotor edge, leaving the rotor area free of mechanical components.

The wind turbine surge and pitch motion is actuated controlling the horizontal position of the prismatic joints A and B. B coincides with the tower base and its position x_2 in the inertial reference frame is the wind turbine surge position. The platform pitch angle β is set controlling the position of A relative to B (i.e., $x_2 - x_1$). The nacelle yaw motion σ is controlled with an actuator placed in correspondence of B and with a rotational axis aligned with l_2. The maximum travel is $\pm$100mm for surge, $\pm 7^\circ$ for pitch and the yaw degree of freedom can perform a 360° rotation.

4.2. Probabilistic multibody model

The robotic platform will be used to simulate motions driven by wave excitation and wind turbulence which are stochastic in nature, thus the most demanding operating condition is unknown. Furthermore, the non-linearity of robot kinematics implies the most challenging operating condition does not arise from aggregating the most demanding conditions for individual degrees of freedom. For this reason, loads for the sizing of the robot actuators and links, and the dimensioning of structural components are carried out with a probabilistic approach.

The probabilistic approach combines a multibody model of the robot created in *Simscape* and the Monte Carlo method. The multibody model is used to solve the inverse dynamic problem in which component-level loads are calculated for several motion conditions with different combinations of platform surge-pitch and nacelle yaw. The robot design approach is iterative: the multibody model is updated with the structural characteristics (geometry, mass properties, elastic properties) of components that are dimensioned with the results of simulations until the final configuration is reached.

The Monte Carlo method is applied simulating a number of scenarios N where a sinusoidal

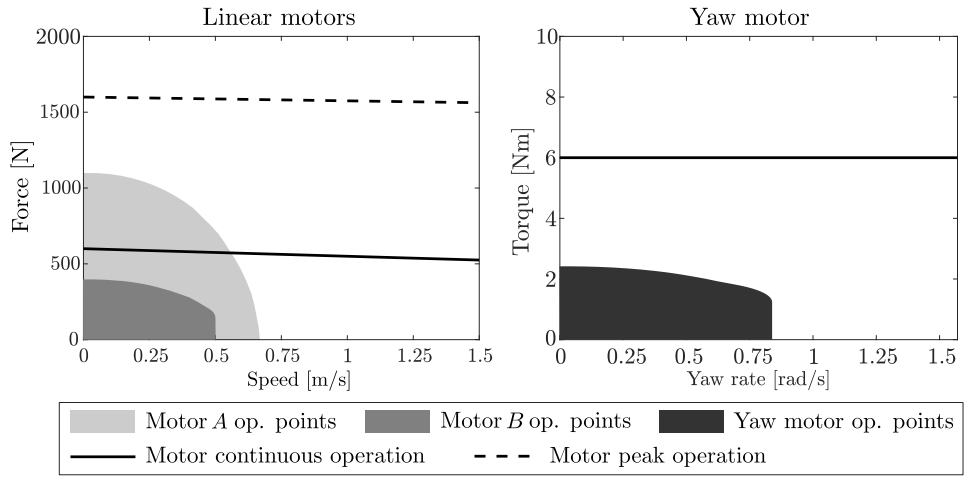

Figure 5. Load-speed requirements for the actuators of the robotic platform that are obtained from the probabilistic multibody model are compared to specifications of the motors selected for the final design.

motion as in Eq. 1 is prescribed to the surge, pitch, and the nacelle yaw degrees of freedom. $A_{\mathrm{m},0}$, f_{m} and φ_{m} are drawn from their probability distribution functions

$$f_{\mathrm{m}} \sim \mathcal{U}_{[0,f_{\mathrm{m,max}}]}\,, \quad \varphi_{\mathrm{m}} \sim \mathcal{U}_{[-\pi,\pi]}\,, \quad A_{\mathrm{m},0} \sim \mathcal{U}_{[-0.9\xi_{\mathrm{max}},0.9\xi_{\mathrm{max}}]}\,, \tag{4}$$

where ξ_{max} is the maximum travel allowed for the ξ degree of freedom. For any f_{m}, the corresponding value of A_{m} is obtained interpolating the amplitude-frequency mappings of Fig. 2. In the simulations, the rotor speed is set to rated, the aerodynamic loading on the rotor is modeled with constant thrust force and torque applied at the rotor hub (torque values are reported in Table 2, the thrust force is [19, 30, 42]N for the 10MW, 15MW, and 22MW scale models respectively).

Figure 5 shows the load requirements for the robot actuators obtained from $N = 100$ runs of the multibody probabilistic model. Linear motors are placed in correspondence of joints A and B and produce a foce in the x direction, the yaw motor is positioned in B and generates a torque in the direction of the l_2 link. Requirements of individual model runs lie inside the colored areas which are symmetric about the plot axes. Motor A is responsible for controlling the pitch motion of the wind turbine, requiring it to develop a force that is more than double that of motor B, which solely acts on the surge motion. The multibody model shows that loads for linear motors are mostly driven by inertia of the wind turbine components. The peak yaw torque is about 2Nm and is mostly due to nacelle inertia and the rotor gyroscopic moment.

5. Final design of the Robot

The final layout of the robot is displayed in Fig. 6. The system can be divided in two subsystems, the rotor-nacelle assembly and the robotic platform, that are connected with a flanged tube which constitutes the upper portion of the tower. The lower portion of the tower is the link l_2.

The linear actuators in the joints A and B are two brushless linear servo motors, which force characteristic is shown in Fig. 5. As visible, the selected motors are able to cover peak loads in all scenarios defined with the Monte Carlo approach. Some conditions are above the continuous operation threshold for the A actuator, but this is deemed acceptable because wind tunnel tests are carried out in an intermittent way.

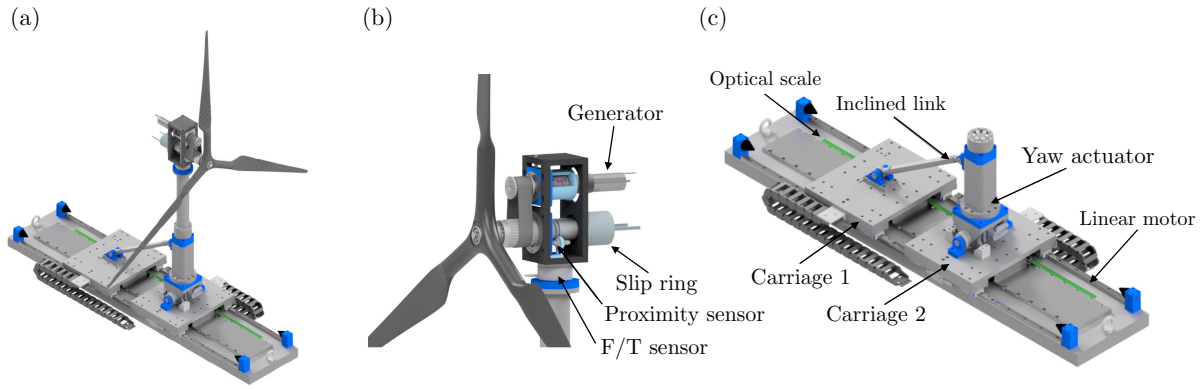

Figure 6. Overview of the wind turbine on top of the robotic platform. **(a)** complete assembly. **(b)** rotor-nacelle assembly (F/T sensor is the 6-components load cell). **(c)** robotic platform.

The wind turbine nacelle is structured with two parallel shafts connecting the generator to the rotor. The lower shaft is hollow and allows the passage of electric cables or a coaxial shaft needed to realize pitch controls in future versions of the wind turbine. The nacelle-yaw actuator, a Harmonic Drive FHA-C Mini, is placed in correspondence of joint B. The yaw motor shaft rotates inside the link l_2 which is realized with a hollow sleeve and is connected to the rest of the turbine tower just above the joint C. Modularity in wind turbine dimensions is achieved replacing the flanged tube and the wind turbine rotor.

5.1. Generator and transmission

The generator is an electric motor that fits the torque and power requirements defined in Sect. 3.2. In addition to the gearbox reduction $\tau_g = 14{:}1$, the belt introduces a reduction factor of $\tau_b = 1.36{:}1$, hence the total transmission ratio is $\tau_{gb} = 19.04{:}1$. The gearbox efficiency is $\eta_g = 0.8$, the efficiency of the belt transmission is $\eta_b = 0.96$, thus the overall transmission efficiency is equal to $\eta_{gb} = 0.77$. The motor is a Maxon EC-4pole-30 of 200W power that provides a maximum rotor speed of 840rpm and a nominal braking torque at rotor of 2204mNm. The electric motor is controlled by a Maxon ESCON 70/10 and is operated as a generator. It can be controlled in speed, with a user defined speed set point, or in torque, and the torque set point is computed with the wind turbine control strategy as discussed in [10].

5.2. Sensors

The robot integrates sensors to measure the wind turbine motions and loads. Generator speed necessary for wind turbine control is measured with the encoder ENC 16 EASY that is embedded in the generator. Positions of the joints A and B, utilized to control the robot motion, are measured by means of a Heidenhain LIC 2117 exposed linear encoder with an accuracy of 15μm and a resolution of 50nm: they corresponds to an accuracy of 8m° and a resolution of 0.04m° for the pitch degree of freedom. The sensor performance covers the requirements for testing with stochastic waves of Fig. 3 with margin for other floating platform concepts or operational sea conditions characterized by smaller amplitudes of motions. Large motions are resolved with the same accuracy of very small ones since the sensor accuracy is constant throughout its measurement range. The surge and pitch position is computed from the position of joints A and B solving the direct kinematics of the robot. The base of the nacelle structure is fixed to an ATI Mini58 6-components load cell that measures forces and moments acting on the nacelle and on the rotor.

6. Conclusions

Experiments in a controlled environment like a wind tunnel can be leveraged to improve our understanding of wind turbine wakes and their interaction with rotors in floating wind farms. Experiments must replicate with good accuracy the physics of atmospheric wind and the motion of the floating foundation and one key element to achieve this degree of fidelity is the robotic platform moving wind turbines in the wind tunnel. In this paper, we examine the increasingly stringent requirements that the robotic system must meet, surpassing those applicable to individual turbine testing conducted in previous studies. The robot has small size to avoid obstructing the flow inside the farm, to recreate the coupling between rotor and atmospheric wind, and to place multiple wind turbine units inside the wind tunnel test section. It moves the wind turbine in the platform surge and pitch directions up to 10Hz, reaching accelerations up to 40 $\mathrm{m\,s^{-2}}$. At the same time, thanks to the combination of special sensors and a parallel kinematic structure, it has very accurate positioning performance needed to replicate at small scale motions due to irregular waves in 10-22MW floating wind turbines.

Acknowledgements

This study was carried out within the NEST - Network 4 Energy Sustainable Transition (D.D. 1243 02/08/2022, PE00000021) and received funding under the National Recovery and Resilience Plan (NRRP), Mission 4 Component 2 Investment 1.3, funded from the European Union - NextGenerationEU. This manuscript reflects only the authors' views and opinions, neither the European Union nor the European Commission can be considered responsible for them.

References

[1] Meyers J, Bottasso C, Dykes K, Fleming P, Gebraad P, Giebel G, Göçmen T and van Wingerden J W 2022 *Wind Energy Science* **7** 2271–2306 URL https://wes.copernicus.org/articles/7/2271/2022/

[2] Fontanella A, Bayati I, Mikkelsen R, Belloli M and Zasso A 2021 *Wind Energy Science* **6** 1169–1190 URL https://wes.copernicus.org/articles/6/1169/2021/

[3] Bergua R, Robertson A, Jonkman J, Branlard E, Fontanella A, Belloli M, Schito P, Zasso A, Persico G, Sanvito A, Amet E, Brun C, Campaña Alonso G, Martín-San-Román R, Cai R, Cai J, Qian Q, Maoshi W, Beardsell A, Pirrung G, Ramos-García N, Shi W, Fu J, Corniglion R, Lovera A, Galván J, Nygaard T A, dos Santos C R, Gilbert P, Joulin P A, Blondel F, Frickel E, Chen P, Hu Z, Boisard R, Yilmazlar K, Croce A, Harnois V, Zhang L, Li Y, Aristondo A, Mendikoa Alonso I, Mancini S, Boorsma K, Savenije F, Marten D, Soto-Valle R, Schulz C W, Netzband S, Bianchini A, Papi F, Cioni S, Trubat P, Alarcon D, Molins C, Cormier M, Brüker K, Lutz T, Xiao Q, Deng Z, Haudin F and Goveas A 2023 *Wind Energy Science* **8** 465–485 URL https://wes.copernicus.org/articles/8/465/2023/

[4] Cioni S, Papi F, Pagamonci L, Bianchini A, Ramos-García N, Pirrung G, Corniglion R, Lovera A, Galván J, Boisard R, Fontanella A, Schito P, Zasso A, Belloli M, Sanvito A, Persico G, Zhang L, Li Y, Zhou Y, Mancini S, Boorsma K, Amaral R, Viré A, Schulz C W, Netzband S, Soto-Valle R, Marten D, Martín-San-Román R, Trubat P, Molins C, Bergua R, Branlard E, Jonkman J and Robertson A 2023 *Wind Energy Science* **8** 1659–1691 URL https://wes.copernicus.org/articles/8/1659/2023/

[5] Fontanella A, Facchinetti A, Daka E and Belloli M 2023 *Renewable Energy* **219** 119442 ISSN 0960-1481 URL https://www.sciencedirect.com/science/article/pii/S0960148123013575

[6] Messmer T, Brigden C, Peinke J and Hölling M 2022 *Journal of Physics: Conference Series* **2265** 042015 URL https://dx.doi.org/10.1088/1742-6596/2265/4/042015

[7] Bak C, Bitsche R, Yde A, Kim T, Hansen M, Zahle F, Gaunaa M, Blasques J, Døssing M, Wedel Heinen J J and Behrens T 2012 Light Rotor: The 10-MW reference wind turbine *Proceedings of EWEA 2012 - European Wind Energy Conference & Exhibition* (European Wind Energy Association (EWEA)) eWEC 2012 - European Wind Energy Conference & Exhibition, EWEC 2012 ; Conference date: 16-04-2012 Through 19-04-2012 URL http://events.ewea.org/annual2012/

[8] Gaertner E, Rinker J and Sethuraman L, Zahle F, Anderson B, Barter G, Abbas N, Meng F, Bortolotti P, Skrzypinski W, Scott G, Feil R, Bredmose H, Dykes K, Shields M, Allen C and Viselli A 2020 Available at https://www.nrel.gov/docs/fy20osti/75698.pdf URL https://www.nrel.gov/docs/fy20osti/75698.pdf

[9] IEA-22-280-RWT. Repository for 22MW offshore reference wind turbine https://github.com/IEAWindTask37/IEA-22-280-RWT accessed: 2023-12-12

[10] Fontanella A, Da Pra G and Belloli M 2023 *Energies* **16** ISSN 1996-1073 URL https://www.mdpi.com/1996-1073/16/5/2205
[11] Schulz C W, Netzband S, Özinan U, Cheng P W and Abdel-Maksoud M 2024 *Wind Energy Science* **9** 665–695 URL https://wes.copernicus.org/articles/9/665/2024/
[12] Lemmer F, Raach S, Schlipf D, Faerron-Guzmán R and Cheng P W 2020 FAST model of the SWE-TripleSpar floating wind turbine platform for the DTU 10MW reference wind turbine URL https://doi.org/10.18419/darus-514
[13] Allen C, Viselli A, Dagher H, Goupee A, Gaertner E, Abbas N, Hall M and Barter G Definition of the UMaine VolturnUS-S reference platform developed for the IEA Wind 15-megawatt offshore reference wind turbine Tech. rep. International Energy Agency